FESI Publishing

Supplement to Proceedings

ESIA 14 , ISSI 2017

Edited by B. Tomkins and S.-T. Tu

The Treatment of Bending Stress Due to Internal Pressure at Nozzle Crotch Corner of Pressure Vessel for Defect Tolerance Assessment

K. Miyazaki, F. Iwamatsu, F. Hirokawa, and M. Masuda

The Evaluation of Remaining Strength for T-Joint Piping with Fully Circumferential Local Wall Thinning Subjected to Internal Pressure

K. Miyazaki and T. Takayanagi

The Treatment of Bending Stress Due to Internal Pressure at Nozzle Crotch Corner of Pressure Vessel for Defect Tolerance Assessment

K. Miyazaki[1,*], F. Iwamatsu[2], F. Hirokawa[3], and M. Masuda[3]

Abstract. — The bending stress through the thickness of a pressure vessel due to internal pressure is classified as secondary stress, which does not contribute to plastic collapse, in ASME Section III. However, the R6 procedure for defect tolerance assessment (DTA) states that the stresses produced by external loads, such as pressure, are categorised as primary stresses and not contributing to plastic collapse. In order to clarify the treatment of bending stress due to internal pressure at the nozzle crotch corner of a pressure vessel for DTA, elastic-plastic finite element analyses (FEA) were conducted. Since the bending stress component through the thickness gradually disappeared with increasing internal pressure in a non-flawed model, the bending stress could be treated as the secondary stress. Further, the yield pressures of vessels with a nozzle were estimated by FEA and the plastic collapse parameter L_r of a plate model in the R6 procedure with bending stress was categorised as primary or secondary stress. It was confirmed that the classification of bending stress due to internal pressure as secondary stress is suitable for DTA.

I. Introduction

Since high structural integrity is required for pressure vessels, the American Society of Mechanical Engineers established Boiler and Pressure Vessel Code Section III (ASME Section III) containing rules for construction of nuclear facility components (*1*). The ASME Section III requires the categorisation of stresses obtained through the stress analysis as primary, secondary, and peak. Especially, primary stresses contribute to plastic collapse and secondary stresses do not affect plastic collapse. For example, the membrane stress due to internal pressure is categorised as primary stress. However, the bending stress through the thickness due to internal pressure is categorised as secondary stress according to ASME Section III. On the other hand, since the quantification of allowable defects at the start of plant life is required by the UK nuclear regulation, the sophisticated elastic-plastic fracture mechanics defect tolerance assessment (DTA) should be conducted according to the R6 procedure (*2*). The plastic collapse parameter L_r, which is defined as the ratio of applied load to plastic collapse load, should be calculated with only primary stresses according to R6. In the R6 procedure, primary stress is defined as all stresses arising from external loads that contribute to plastic collapse such as internal pressure. There are discrepancies in stress categorisation between ASME Section III and the R6 procedure.

[1] *Saiwai-cho 3-1-1, Hitachi, Ibaraki, Japan; Hitachi Works, Hitachi-GE Nuclear Energy, Ltd.*
[2] *Omika-cho 7-1-1, Hitachi, Ibaraki, Japan; Research and Development Group, Hitachi, Ltd.*
[3] *Omika-cho 5-2-2, Hitachi, Ibaraki, Japan; Hitachi Works, Hitachi-GE Nuclear Energy, Ltd.*
* Corresponding Author

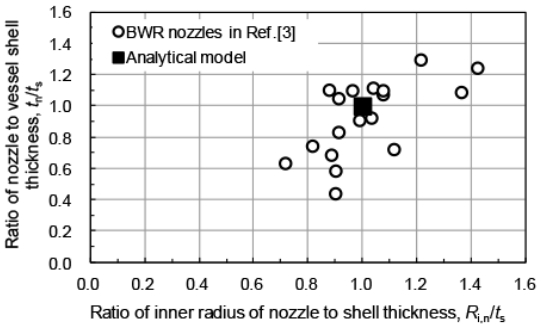

FIG. 1. — Nozzle geometries of BWR nozzles and analytical model.

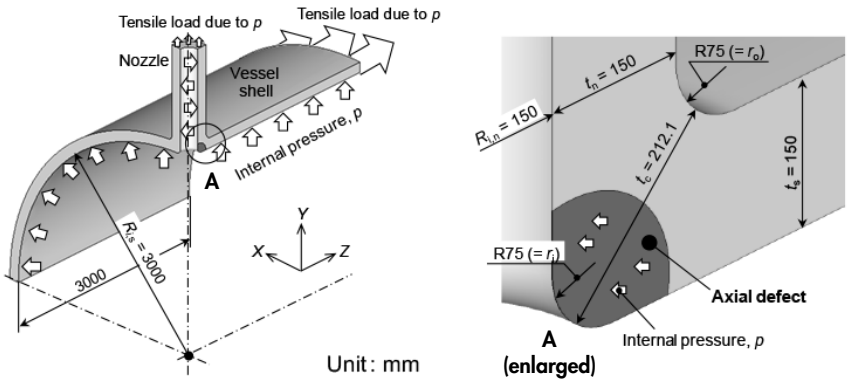

FIG. 2. — 3D model of the nozzle crotch corner in a pressure vessel.

In order to clarify the stress categorisation, especially treatment of bending stress due to internal pressure for DTA at the nozzle crotch corner of a pressure vessel, the variation in the stress distribution with increasing internal pressure and yield pressure were estimated by elastic-plastic finite element analysis (FEA).

II. Analysis Conditions

Walter and Sommerville (*3*) analysed the stress correction factors of nozzles in 18 boiling water reactors (BWR). The relationship between the ratio of the inner radius of nozzle to vessel shell thickness $R_{i,n}/t_s$, and that of nozzle to vessel shell thickness t_n/t_s from their survey results, are shown in Fig. 1. Considering the tendency of BWR nozzle geometries, an analytical model with $R_{i,n}/t_s = 1.0$ and $t_n/t_s = 1.0$ was determined, as shown in Fig. 1. A 3D model of the nozzle crotch corner in a pressure vessel is shown in Fig. 2. A quarter of the pressure vessel with a nozzle was characterised by considering the symmetrical conditions. The inner radius $R_{i,s}$, t_s, and length of the vessel shell are 3,000,

150, and 3,000 mm, respectively. The $R_{i,n}$, t_n are 150 mm, and the inner and outer radii of the nozzle crotch corner r_i and r_o are 75 mm. To simulate the internal pressure, the analytical model was subjected to both pressure loading at the inside of the model and tensile loading due to internal pressure at the end of the nozzle and shell.

An axial defect was assumed in order to take into account the principal stress direction due to internal pressure at inside of the nozzle crotch corner, as shown in Fig. 2. The geometries of an axial defect at the nozzle crotch corner are defined in Fig. 3. The shape of the defect front line forms a part of an ellipse, with the centre location coincident with the crotch corner centre. The depth direction of the defect is 45° to the axial direction of the shell. The aspect ratio of the elliptical defect, which is defined as the ratio of the depth a to the length l of the defect, is 0.5. The defect length is defined as the length perpendicular to the depth direction in the assumed plate with $t_c = 212.1$ mm, which is equivalent to the distance from inside to outside of the nozzle crotch corner, as shown in Fig. 3. The dimensions of the vessel shell, nozzles and defect depth are listed in the table. The defect depths a varied from 10 through to 120 mm, and are equivalent to a/t_n or $a/t_s = 0.07$ to 0.80 and $a/t_c = 0.05$–0.57. In addition, a non-flawed shell model was also analysed to understand the basic tendency of variation in stress distribution due to the increase in internal pressure.

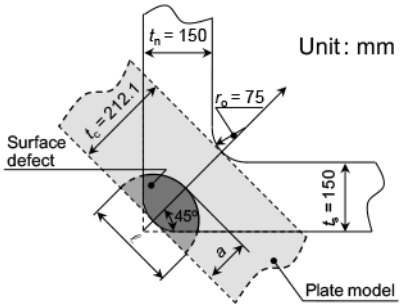

FIG. 3. — Definition of defect geometry at the nozzle crotch corner.

The material of a pressure vessel with a nozzle is low-alloy forging material, SA-533B Class 1, and the properties are based on ASME Boiler and Pressure Vessel Code Section II (*4*). The assumed stress–strain curve for application of FEA is shown in Fig. 4. Considering the assumed operating temperature (54 °C = 130 °F), the yield stress σ_Y and Young's modulus E is 337 MPa and 189 GPa, respectively. Although the plastic collapse is calculated based on the assumption of ideal elastic-plastic behaviour of the material, the bilinear stress–strain curve, the second slope E' which is equivalent to E/1,000, is used by considering the convergence of analysis. By using elastic-plastic FEA with ABAQUS version 6.13–5, the stress and strain of a pressure vessel model with a nozzle due to an increase in internal pressure were estimated.

III. Stress Distribution Through the Thickness at the Nozzle Crotch Corner Due to Internal Pressure

The von Mises stress contours around the nozzle crotch corner due to internal pressure are shown in Fig. 5. The yielding zone propagated from the inside of the nozzle crotch corner with an increase in internal pressure in the case of flawed models with $a = 20$, 40, and 100 mm ($a/t_n = 0.09$, 0.19, and 0.47) as well as of non-flawed models. In addition, the

TABLE

Shell and nozzle geometries and defect depths.

Case No.	Shell geometry		Nozzle geometry		Thickness at nozzle corner, t_c (mm)	Defect depth		
	Inner radius, $R_{i,s}$ (mm)	Thickness, t_s (mm)	Inner radius, $R_{i,n}$ (mm)	Thickness, t_n (mm)		a (mm)	a/t_s or a/t_n	a/t_c
N-0	3,000	150	150	150	212.1	0	0.00	0.00
N-1						10	0.07	0.05
N-2						20	0.13	0.09
N-3						40	0.27	0.19
N-4						60	0.40	0.28
N-5						80	0.53	0.38
N-6						100	0.67	0.47
N-7						120	0.80	0.57

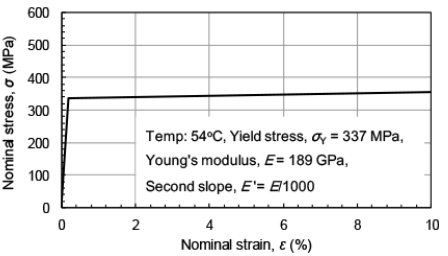

FIG. 4. — Assumed stress–strain curve for application of elastic-plastic FEA.

progress of plasticity from elasticity could be seen not at the nozzle but at the vessel shell and nozzle crotch corner regions.

The hoop stress distributions from inside through outside of the nozzle crotch corner due to internal pressure are shown in Fig. 6. Although the hoop stresses occurred in the perpendicular direction of the axial defect and the membrane stress component increased due to the increase in internal pressure, the bending stress component disappeared after yielding in the non-flawed model as shown in Fig. 6a. The same tendency could be seen in the flawed models with $a = 20$ or 40 mm ($a/t_c = 0.09$ and 0.19) on the ligament of the flawed section except for the defect tip, as shown in Fig. 6b and 6c. From these behaviours of hoop stress distribution for the non-flawed or shallow flawed models, it is simply judged that the bending stress component due to internal pressure could be treated as secondary stress.

On the other hand, the hoop stress and membrane stress component increased and bending stress component did not disappear for the deep flawed model with $a = 100$ mm ($a/t_c = 0.47$), as shown in Fig. 6c. For a deeper discussion, the von Mises stress contours at the yield pressure for the deep flawed model with $a = 100$ mm is shown in Fig. 7. The yield pressure p_Y is defined as the pressure in case that the yielding zone extends from

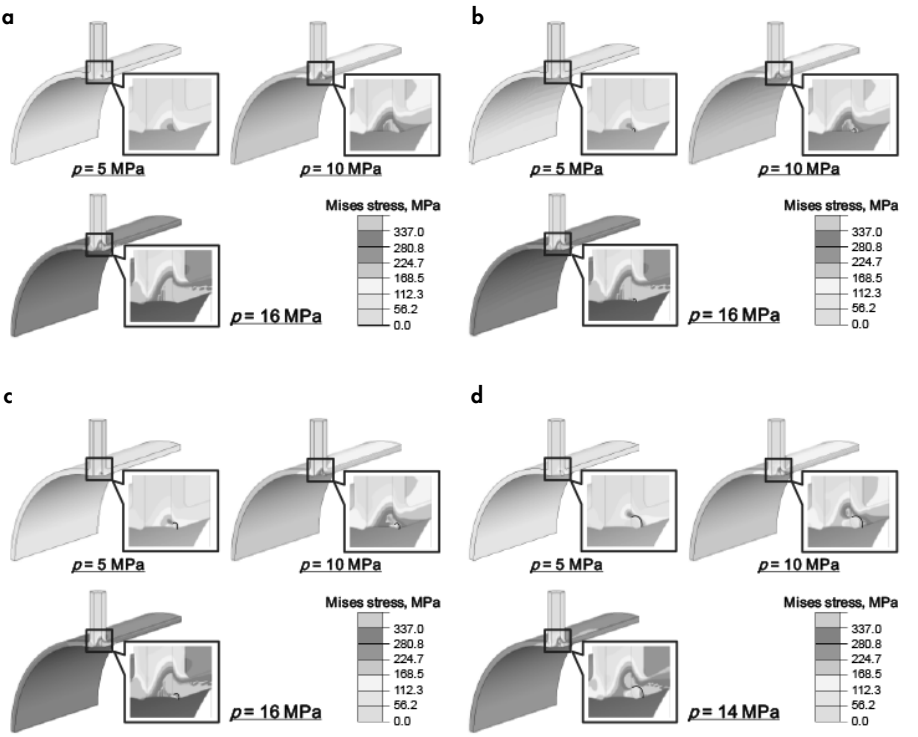

FIG. 5. — von Mises stress contours around the nozzle crotch corner due to internal pressure. *a*. Non-flawed model. *b*. Flawed model with $a = 20$ mm ($a/t_n = 0.09$). *c*. Flawed model with $a = 40$ mm ($a/t_n = 0.19$). *d*. Flawed model with $a = 100$ mm ($a/t_n = 0.47$).

inside to outside of the pressure vessel model by FEA. Although the hoop stress distributions from inside through outside of the nozzle crotch corner were compared in Fig. 6, the collapse section was not the ligament of the flawed nozzle crotch corner but the shell region close to the nozzle. The representative equivalent von Mises stress distributions from the deepest point of a defect to the outside evaluation point at the collapse section in case of $a = 100$ mm ($a/t_c = 0.47$) are shown in Fig. 8. Since the bending stress component disappeared with an increase in internal pressure after yield, the bending stress component could be classified as secondary stress at the collapse section.

As mentioned previously, the bending stress component did not disappear for the deep flawed model with $a = 100$ mm ($a/t_c = 0.47$) at the ligament of the nozzle crotch corner, as shown in Fig. 6c. Although it seems that the bending stress occurred locally to balance the deformation between the vessel shell and high rigid nozzle due to the structural discontinuity at the ligament of the deep flawed section, the classification of the bending stress component due to internal pressure as primary stress seems a conservative assumption in calculating the plastic collapse parameter L_r. Classifying bending stress component due to internal pressure as secondary stress will be discussed through the comparison

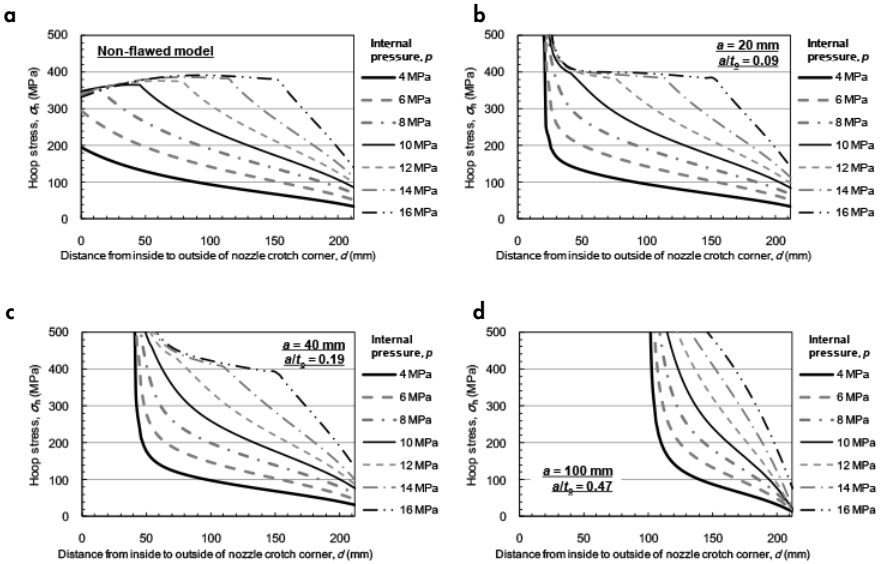

FIG. 6. — Hoop stress distributions from inside through outside of the nozzle crotch corner due to internal pressure. *a*. Non-flawed model. *b*. Flawed model with $a = 20$ mm ($a/t_c = 0.09$). *c*. Flawed model with $a = 40$ mm ($a/t_c = 0.19$). *d*. Flawed model with $a = 100$ mm ($a/t_c = 0.47$).

of the yield pressures p_Y calculated using simplified L_r solution in the R6 procedure and those estimated from FEA in the next section.

III. Comparison of the Yield Pressure Estimated Using Simplified Solution of Plastic Collapse Parameter and Finite Element Analysis

The plastic collapse parameter L_r is defined in the R6 procedure (*2*) as

(1) $$L_r = \frac{\sigma_m}{(\sigma_m(\lambda))_L} \quad , \quad \lambda = \frac{1}{6}\frac{\sigma_b}{\sigma_m} \quad ,$$

where $(\sigma_m(\lambda))$ is the limit membrane stress, and σ_m and σ_b are the uncracked body membrane and bending stresses, respectively. The normalised limit force n_L is also defined as

(2) $$n_L = \frac{(\sigma_m(\lambda))_L}{\sigma_Y} \quad ,$$

where σ_Y is yield stress. When the pressure vessel reaches the yielding condition, the following equation is established,

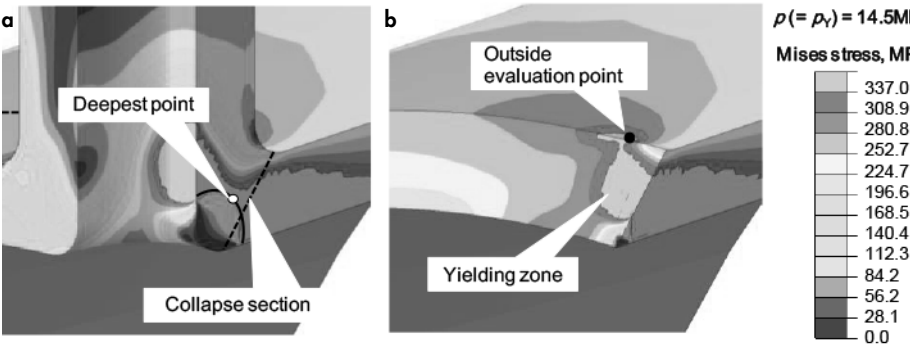

FIG. 7. — von Mises stress contours at the yield pressure p_Y for a deep flawed model with $a=100$ mm ($a/t_c=0.47$). *a*. Nozzle corner region. *b*. Nozzle cutting model at the collapsed section.

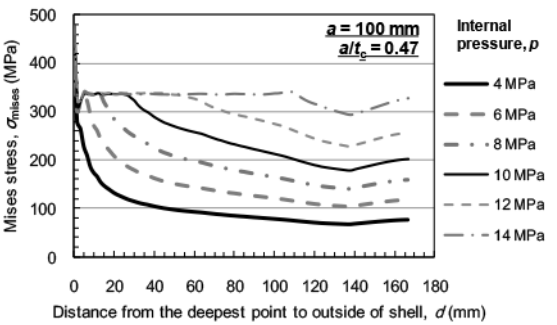

FIG. 8. — von Mises stress distribution from the deepest point to outside evaluation point at collapse section for flawed model with $a=100$ mm ($a/t_c=0.47$).

$$L_{r,Y}(p=p_Y)=\frac{\sigma_{mY}}{(\sigma_m(\lambda))_L}=\frac{\sigma_{mY}}{n_L\sigma_Y}=1.0 \quad , \quad \therefore \sigma_{mY}=n_L\sigma_Y \quad , \tag{3}$$

where σ_{mY} is the uncracked body membrane stress at the yield condition. In addition, when the pressure vessel is subjected to the standard internal pressure p_0 and the uncracked body standard membrane stress σ_{m0} occurred, σ_{mY} is represented as

$$\sigma_{mY}=\frac{p_Y}{p_0}\,\sigma_{m0} \tag{4}$$

From Eq. (3) and Eq. (4), the failure pressure can be estimated simply as

$$\therefore p_Y=\frac{n_L\sigma_Y}{\sigma_{m0}}\,p_0 \tag{5}$$

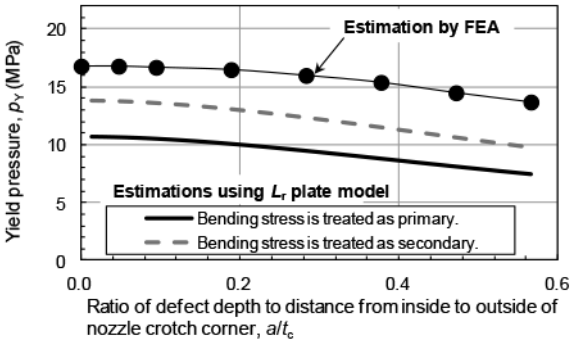

FIG. 9. — Comparison of yield pressures p_Y estimated from L_r parameter for plate model and FEA.

The n_L is given in the R6 procedure and the nozzle crotch corner can be characterised as the plate model with a thickness t equivalent to the distance from the inside to the outside of the nozzle crotch corner, $t_c = 212.4$ mm, as shown in Fig. 3.

The relationship between the p_Y and a/t_c is shown in Fig. 9. The yield pressures p_Y were estimated using Eq. (5) with the L_r plate model. When applying the L_r plate model, the bending stress component due to internal pressure was treated as primary or secondary stress. As mentioned previously, p_Y is defined as the pressure when the yielding zone extends from the inside to the outside of the pressure vessel model through FEA. The p_Y values estimated through FEA were higher than those calculated using the L_r plate model, when the bending stress component was classified as both primary and secondary. In addition, the p_Y values calculated when the bending stress was classified as secondary stress were closer to those estimated through FEA than those calculated when the bending stress component was classified as primary stress.

From direct comparison of the estimated yield pressure, it is judged that the classification of the bending stress component due to internal pressure at the nozzle crotch corner as secondary stress is suitable for the estimation of L_r in DTA.

IV. Summary

In order to clarify the stress categorisation, especially in the treatment of bending stress due to internal pressure for DTA at the nozzle crotch corner of a pressure vessel, the variation of stress distribution with an increase of internal pressure and yield pressure were estimated through elastic-plastic FEA.

Although hoop stresses occurred in the perpendicular direction of the axial defect and membrane stress increased due to an increase in internal pressure, the bending stress component disappeared after yield for the non-flawed and shallow flawed models. From these behaviours, it is judged that the bending stress component due to internal pressure may be treated as secondary stress. Since the bending stress component disappeared with an increase in internal pressure for the deep flawed model after yield at the collapse

section, it may be concluded that the bending stress component also manifested secondary stress behaviour for deep flawed models.

Classification of the bending stress component due to internal pressure at the nozzle crotch corner as secondary stress is suitable for the estimation of L_r in DTA from direct comparison of estimated yield pressure p_Y.

References

1. ASME, "ASME Boiler and Pressure Vessel Code (BPVC) Section III — Rules for Construction of Nuclear Facility Components". American Society of Mechanical Engineers, New York, NY, USA, 2015.
2. EDF Energy, "Assessment of the Integrity of Structures Containing Defects, R6 Revision 4: Addendum 11." EDF Energy, Gloucester, UK, 2015.
3. M. C. Walter and D. V. Sommerville, "Nozzle Blend Radius Peak Stress Correction Factors for 2-D Axisymmetric Finite Element Models" *in* "Proceedings" American Society of Mechanical Engineers (ASME) 2010 Pressure Vessels and Piping Conference, Bellevue, Washington, USA, 18th–22nd July 2010. Volume 3, Paper No. PVP2010-25104, pp. 317–25.
4. ASME, "ASME Boiler and Pressure Vessel Code (BPVC) Section II — Materials, Part D: Properties." American Society of Mechanical Engineers, New York, NY, USA, 2015.

The Evaluation of Remaining Strength for T-Joint Piping with Fully Circumferential Local Wall Thinning Subjected to Internal Pressure

K. Miyazaki* and T. Takayanagi

Abstract. — Although the evaluation procedures of allowable local wall thinning depth and remaining strength for pressurised components are provided in fitness-for-service codes, such as API579-1, BS7910, and ASME B31G, the applicability of procedures to the fitting of pipes with local wall thinning is unclear. In order to clarify the applicability of current procedures to T-joint pipes with fully circumferential local wall thinning subjected to internal pressure, finite element analyses (FEA) were conducted. The failure pressures of T-joint pipe were affected by the geometry of local wall thinning. However, the failure pressures of T-joint pipes were much higher than the allowable design pressure with a constant minimum thickness assumption in the design code. In addition, the remaining strength factors (*RSF*), defined as the ratio of the failure pressure of T-joint pipes with local wall thinning to that of pipes without wall thinning, were estimated by FEA and were compared with those in fitness-for-service codes. It was clarified that API579-1 generally gave good estimations of *RSF* for T-joint pipes with local wall thinning except for deep and narrow ones.

I. Introduction

Wall thinning due to flow-accelerated corrosion is assumed to occur in pressurised piping systems of power plants and chemical plants, etc. In order to manage the wall thinning of piping systems, the Japan Society of Mechanical Engineers (JSME) maintains the rules on pipe wall thinning management for light water reactors (*1*,*2*). The JSME rules on pipe wall thinning estimate the allowable thickness of local wall thinning on the basis of an assumption of constant thickness as general corrosion; however, the allowable thickness is too thick for local wall thinning. On the other hand, the estimation procedures for allowable local wall thinning depth and remaining strength as acceptance standards for pressurised components are provided in fitness-for-service codes such as API579-1 (*3*), BS7910 (*4*), and ASME B31G (*5*) in order to manage degraded piping systems. Although the acceptance standards for local wall thinning in fitness-for-service codes were developed through experimental and analytical discussions for mainly straight pipes, the pertinence of acceptance standards for the fitting of pipes such as T-joint pipes with local wall thinning is unclear.

In order to clarify the bearing of current acceptance standards to T-joint pipes with fully circumferential local wall thinning subjected to internal pressure, the failure pressures of T-joint pipes were estimated by finite element analyses (FEA).

Saiwai-cho 3-1-1, Hitachi, Ibaraki, Japan/Hitachi Works, Hitachi-GE Nuclear Energy, Ltd.

* Corresponding Author

II. Analytical Conditions

The physical properties of the T-joint pipe are shown in Fig. 1. The outer diameter, D_o, and the nominal thickness, T, of both schedule 160 run and branch pipes—whose nominal size is 10 in—were 267.4 mm and 28.6 mm, respectively. The lengths of the run and branch pipes were three times that of the outer diameter, i.e. $3D_o$. The radius of the crotch corner R_o was 57 mm. There is a fully circumferential local wall thinning at the crotch corner of the T-joint pipes. The dimensions of T-joint pipes and the geometry of local wall thinning are listed in Table I. The ratios of the thickness of local wall thinning to that of nominal thickness T'/T are 0.8, 0.5, and 0.2. The angles 2θ of local wall thinning were 30°, 60°, and 90°. In addition, an idealised T-joint pipe without wall thinning (case number Tj-L0) was analysed. Since the T-joints were subjected to only internal pressure, a quarter of the models were used for analysis by considering the symmetrical boundary conditions.

The T-joint pipes were made of carbon steel pipes for high-temperature service, STPT410 in Japanese Industrial Standards, JIS G 3456 (*6*), equivalent to ASTM A106, grade B (*7*). The specified minimum yield stress S_Y and ultimate strength S_u at room temperature are 245 MPa and 410 MPa, respectively. API579-1 (*3*) gives an estimation procedure of the relationship between true stress σ_t and true strain ε_t with yield stress σ_Y and ultimate tensile strength σ_u as follows,

$$\varepsilon_t = \frac{\sigma_t}{E} + \left(\frac{\sigma_t}{H_{RO}}\right)^{\frac{1}{n_{RO}}} \tag{1}$$

$$H_{RO} = \frac{\sigma_u \exp(n_{RO})}{{n_{RO}}^{n_{RO}}}, \quad n_{RO} = \frac{1 + 1.3495\left(\frac{\sigma_Y}{\sigma_u}\right) - 5.3117\left(\frac{\sigma_Y}{\sigma_u}\right)^2 + 2.9643\left(\frac{\sigma_Y}{\sigma_u}\right)^3}{1.1249 + 11.0097\left(\frac{\sigma_Y}{\sigma_u}\right) - 11.7464\left(\frac{\sigma_Y}{\sigma_u}\right)^2},$$

where E is Young's modulus. The true stress and true strain curve was estimated with $\sigma_Y = S_Y = 245$ MPa, $\sigma_u = S_u = 410$ MPa, and $E = 203$ GPa, as shown in Fig. 2.

An example of a mesh division of a T-joint pipe with local wall thinning is shown in Fig. 3. The element was tetrahedral with ten nodes. The pipe was more than three layers thick at the point of local wall thinning as well as in the nominal portion. By using large deformation elastic-plastic finite element analysis (FEA) with ABAQUS version 6.6–6, the stress and strain caused by increments of internal pressure were estimated.

In order to estimate the failure or burst pressure of pipes by FEA, the failure criterion is needed. Teshima and colleagues discussed the failure criterion by the comparison of experimentally obtained burst pressure of T-joint pipes and analytically estimated failure pressure (*8*). They concluded that the burst pressure could be evaluated by comparing the corresponding von Mises stress to the true stress equivalent of the ultimate strength. BS7910 provided the prediction procedure for determining the failure pressure by FEA, and the predicted failure pressure is that which causes the averaged von Mises equivalent stress in the ligament to be equal to the material's true tensile strength by

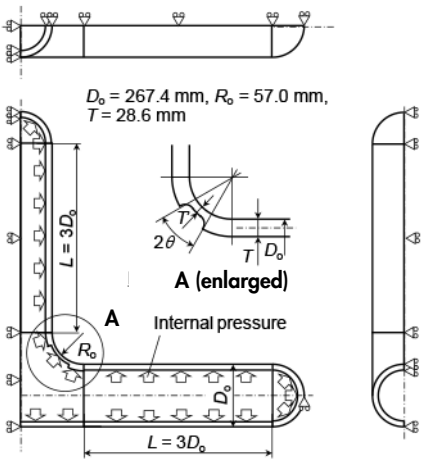

FIG. 1. — Geometry and boundary condition of the T-joint pipe.

means of a uniaxial tensile test (*4*). Taking into account these discussions, the failure pressure was determined as the pressure that causes von Mises stress at the middle thickness point as shown in Fig. 4, which is almost the same as the averaged von Mises

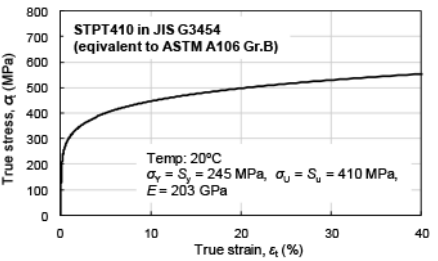

FIG. 2. — Stress–strain curve of STPT410 for FEA.

TABLE I

Dimensions of T-joint pipes and local wall thinnings.

Case No.	Outer diameter, D_o (mm)	Nominal thickness, T (mm)	D_o/T	Outer crotch radius, R_o (mm)	Geometry of local wall thinning		
					2θ (degrees)	T'/T	T' (mm)
Tj-L0	267.4	28.6	9.35	57	0	1.0	28.6
Tj-L1					90	0.8	22.88
Tj-L2						0.5	14.3
Tj-L3						0.2	5.72
Tj-L4					60	0.8	22.88
Tj-L5						0.5	14.3
Tj-L6						0.2	5.72
Tj-L7					30	0.8	22.88
Tj-L8						0.5	14.3
Tj-L9						0.2	5.72

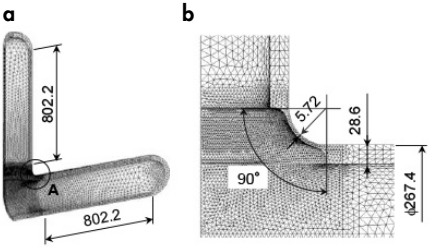

FIG. 3. — Examples of mesh division of T-joint pipes with local wall thinning. *a*. T-joint quarter model. *b*. An enlarged view of the eroded area (A)

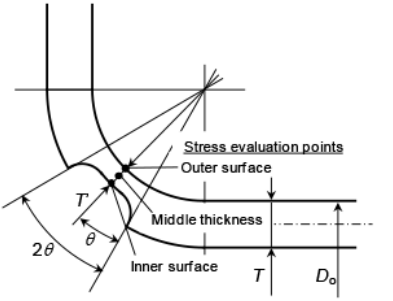

FIG. 4. — Schematic of stress evaluation points at local wall thinning.

stress through the thickness and the membrane stress at the maximum local wall thinning portion, to be equal to the true stress equivalent of the ultimate strength.

III. Analytical Results

Examples of the relationship between von Mises stress and the internal pressure are shown in Fig. 5. Since von Mises stress at the inner surface was higher than those at the middle thickness and the outer surface for case number Tj-4 with $2\theta = 60°$ and $T'/T = 0.8$, the middle thickness gave the averaged von Mises stress through the thickness. The same tendency of von Mises stress with the increment of internal pressure could be seen in almost all of the other cases as shown in Fig. 5a. However, von Mises stress at the outer surface was higher than those at other evaluation points for case number Tj-L6 with $2\theta = 60°$ and $T'/T = 0.2$. The non-negligible local deformation through the thickness occurred at the wall thinning area when deep and shallow metal loss provided the high von Mises stress at the outer surface. In addition, the analytical instability occurred before the von Mises stress at both the middle thickness and the inner surface points reached at the true stress equivalent to σ_u.

The estimated failure pressures of T-joint pipes by FEA are listed in Table II. The allowable pressure $p_{f0,min}$, as defined in ASME Boiler and Pressure Vessel Code Section III (*9*) for calculating the minimum allowable thickness for the pressurised component, is also shown. The $p_{f0,min}$ was estimated as

$$p_{f0,min} = \frac{2T'S}{D_o - 0.8T'} \tag{2}$$

where S is allowable stress and $S = 103$ MPa from ASME Section II (*10*). The margin, defined as the ratio of the failure pressure of T-joint pipes $p_{f,T}$ to allowable pressure $p_{f0,min}$, was much higher than three and depended on the geometry of local wall thinning.

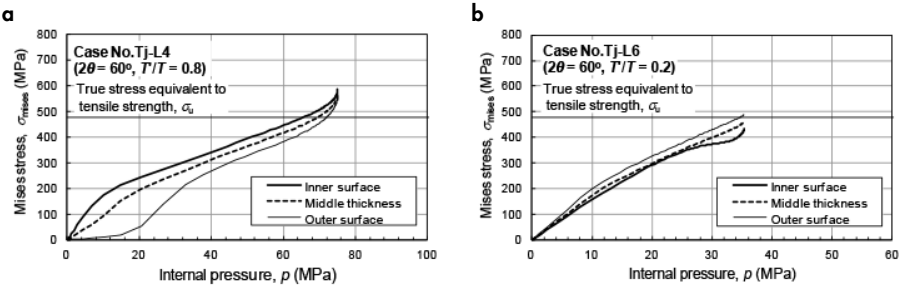

FIG. 5. — Examples of relationship between von Mises stress and internal pressure. *a*. $2\theta = 60°$, $T'/T = 0.8$. *b*. $2\theta = 60°$, $T'/T = 0.2$.

TABLE II

Estimated failure pressures of T-joint pipes by FEA.

Case No.	Wall thinning geometry			Failure pressure, $p_{f,T}$ (MPa) (Stress evaluation point)			Allowable pressure, $p_{f0,min}$ (MPa)	$p_{f,T(middle\ thickness)}/p_{f0,min}$
	2θ (degrees)	T'/T	T' (mm)	Inner surface	Middle thickness	Outer surface		
Tj-L0	0	1.0	28.6	68.5	75.5	78.5	24.1	3.13
Tj-L1	90	0.8	22.9	63.1	68.0	70.2	18.9	3.59
Tj-L2		0.5	14.3	54.2	55.8	55.9	11.5	4.85
Tj-L3		0.2	5.7	32.4<*	32.4<*	31.9	4.5	7.24
Tj-L4	60	0.8	22.9	65.7	69.6	72.0	18.9	3.68
Tj-L5		0.5	14.3	60.4	60.7	60.3	11.5	5.28
Tj-L6		0.2	5.7	35.3<*	35.3<*	34.7	4.5	7.88
Tj-L7	30	0.8	22.9	67.7	72.8	75.3	18.9	3.85
Tj-L8		0.5	14.3	65.7	68.2	69.4	11.5	5.92
Tj-L9		0.2	5.7	36.1	38.5	39.6	4.5	8.58

*Case of occurrence of analytical instability.

The effect of the local wall thinning geometry on the failure pressure of T-joint pipes is shown in Fig. 6. The vertical axis of Fig. 6 shows the remaining strength factor (*RSF*) which is defined as the ratio of the failure pressure of T-joint pipes with local wall thinning $p_{f,T}$ to that without wall thinning $p_{f0,T}$ (= 75.5 MPa). The *RSF* became smaller with a decrease of T'/T and an increment of the wall thinning angle 2θ.

IV. Comparison of Remaining Strength Factors of T-Joint Piping Estimated Analyses and Fitness-For-Service Codes

As mentioned in the previous section, the effect of wall thinning geometry on the failure pressure of T-joint pipes and the *RSF* was recognised. In this section, the *RSF* of T-joint pipes with local wall thinning estimated by FEA are compared with some worldwide codes and standards, which provide the acceptance standards for local wall thinning in piping systems, API579-1, BS7910 and ASME B31G. From these comparisons, the applicability of the current acceptance standards to T-joint pipes with local wall thinning is discussed.

1. Remaining Strength Factors in Fitness-For-Service Codes

API 579-1 (*3*)
API 579-1 provides the direct evaluation procedure of $RSF_{\text{API579-1}}$ as

$$RSF_{\text{API579-1}} = \frac{R_t}{1-\frac{1}{M_t}(1-R_t)} \quad , \quad R_t = T'/T \quad , \tag{3}$$

$$\begin{aligned} M_t = {} & 1.0010 - 0.014195\lambda + 0.2909\lambda^2 - 0.096420\lambda^3 + 0.020890\lambda^4 \\ & - 0.0030540\lambda^5 + 2.9570(10^{-4})\lambda^6 - 1.8462(10^{-5})\lambda^7 + 7.1553(10^{-7})\lambda^8 \\ & - 1.5631(10^{-8})\lambda^9 + 1.4646(10^{-10})\lambda^{10} \quad , \end{aligned}$$

$$\lambda = , \frac{1.285L}{\sqrt{D_i T}}$$

where D_i is the inner diameter and L is the length of wall thinning, which is equivalent to the angle of wall thinning 2θ. Two of the geometric limitations of acceptance standards in API 579-1 are $T'/T \geq 0.20$ and $T' \geq 2.5$ mm.

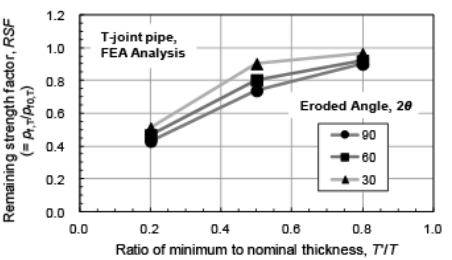

FIG. 6. — Effect of local wall thinning geometry on failure pressure of T-joint pipes.

BS7910 (*4*)
Acceptance of the local wall thinning in pipes is evaluated by the following equations.

$$L_r < L_{r,\max} = \frac{\sigma_Y + \sigma_u}{2\sigma_Y} \quad , \quad L_r = \frac{f_c \sigma_{ref}}{\sigma_Y} \quad , \tag{4}$$

where f_c is the factor of safety and σ_{ref} is the reference stress. From Eq. (4), the boundary of acceptance of local wall thinning is represented as $L_r = L_{r,\max}$. The following equations are given as the boundary of acceptance of local wall thinning with the assumption of a thick wall cylinder and $f_c = 1.0$.

$$\sigma_{ref} = \left[\frac{1-\left(\frac{d}{T}\right)\frac{1}{M}}{1-\left(\frac{d}{T}\right)}\right] \sigma_{h0} = \left[\frac{1-\left(\frac{d}{T}\right)\frac{1}{M}}{1-\left(\frac{d}{T}\right)}\right] \frac{p_{f,BS7910}(D_o - 0.8T)}{2T} = \frac{\sigma_Y + \sigma_u}{2} \quad , \tag{5}$$

$$M = \sqrt{1 + 0.62\{(L/2)^2/(D_o/2)T\}} \quad ,$$

where σ_{h0} is the hoop stress of the nominal portion and $p_{f,BS7910}$ is the estimated failure pressure of pipes with the local wall thinning specified by BS7910. The $p_{f,BS7910}$ is derived from Eq. (5) as follows,

$$p_{f,BS7910} = \frac{(\sigma_Y + \sigma_u)T}{D_o - 0.8T}\left[\left\{1-\left(\frac{d}{T}\right)\right\} \Big/ \left\{1-\left(\frac{d}{T}\right)\frac{1}{M}\right\}\right] \tag{6}$$

On the other hand, the failure pressure of the pipe without local wall thinning $p_{f0,BS7910}$ was estimated with a thick wall cylinder assumption as follows,

$$p_{f0,BS7910} = 2\sigma_u T/(D_o - 0.8T) \tag{7}$$

From Eq. (6) and Eq. (7) the remaining strength factor estimated by BS7910, RSF_{BS7910}, is calculated as follows,

$$RSF_{BS7910} = p_{f,BS7910}/p_{f0,BS7910} = \frac{\sigma_Y + \sigma_u}{2\sigma_u}\left[\left\{1-\left(\frac{d}{T}\right)\right\} \Big/ \left\{1-\left(\frac{d}{T}\right)\frac{1}{M}\right\}\right] \tag{8}$$

One of the geometric limitations of acceptance standards in BS7910 is $T'/T \geq 0.20$.

ASME B31G (*5*)

ASME B31G provides the acceptance standards as the following equation with allowable stress S_F and nominal hoop stress S_o ($=pD_o/2T$ for thin wall cylinder), in the case of the safety factor $SF=1$,

$$S_o < S_F \tag{9}$$

The boundary of acceptance of local wall thinning in B31G was represented as $S_o = S_F$ from Eq. (9). The allowable stress, S_F is given as

$$S_F = S_{flow}\left[\frac{1-0.85(d/T)}{1-0.85(d/T)/M'}\right], \quad S_{flow} = \frac{\sigma_Y+\sigma_u}{2},$$

$$M' = (1+0.6275z-0.003375z^2)^{1/2} \text{ for } z \leqslant 50, \quad M' = 0.032z+3.3 \text{ for } z > 50, \tag{10}$$

$$z = \frac{L^2}{D_oT}$$

From Eq. (10) and the thin wall cylinder assumption, the failure pressure of pipes with local wall thinning by ASME B31G, $p_{f,B31G}$ is estimated as follows,

$$p_{f,B31G} = \frac{2S_FT}{D_o} = \frac{2T}{D_o}\frac{\sigma_Y+\sigma_u}{2}\left[\frac{1-0.85(d/T)}{1-0.85(d/T)/M'}\right] \tag{11}$$

The failure pressure of the nominal pipe without local wall thinning $p_{f0,B31G}$ is estimated with the thin wall cylinder assumption as follows,

$$p_{f0,B31G} = 2\sigma_u T/D_o \tag{12}$$

From Eq. (11) and Eq. (12), the remaining strength factor estimated by ASME B31G, RSF_{B31G}, is calculated as follows,

$$RSF_{B31G} = \frac{p_{f,B31G}}{p_{f0,B31G}} = \frac{\sigma_Y+\sigma_u}{2\sigma_u}\left[\frac{1-0.85(d/T)}{1-0.85(d/T)/M'}\right] \tag{13}$$

One of the geometric limitations of the acceptance standards in ASME B31G is also $T'/T \geqslant 0.20$.

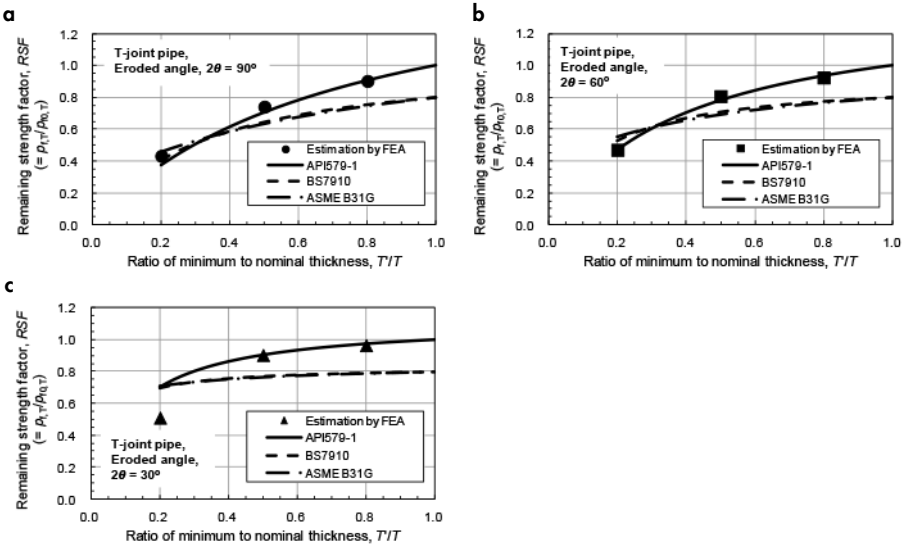

FIG. 7. — Comparison of remaining strength factor for T-joint pipes estimated by FEA and acceptance standards in several fitness-for-service codes. *a*. $2\theta = 90°$. *b*. $2\theta = 60°$. *c*. $2\theta = 30°$.

2. Comparison of Remaining Strength Factors of T-Joint Pipe

The comparison results of *RSF*s of T-joint pipes with local wall thinning estimated by FEA and those by Eq. (3), Eq. (8) and Eq. (13) derived from API579-1, BS7910, and ASME B31G, respectively, are shown in Fig. 7. In the case of the angle of wall thinning $2\theta = 90°$ and 60° as shown in Fig. 7a and Fig. 7b, the acceptance standards in API5791-1 gave the same tendency as *RSF*s estimated by FEA in spite of the difference of the minimum thickness of local wall thinning. Although the *RSF*s estimated by BS7910 and ASME B31G showed the same tendency, they gave lower *RSF*s than those estimated by FEA with an increase in the thickness of local wall thinning. Especially, when T'/T was close to unity, the *RSF* did not come close to unity. It seems that the reason why BS7910 and ASME B31G gave lower *RSF*s is caused by the difference of allowable stress between σ_u for nominal pipe and flow stress defined as the average of σ_Y and σ_u for a pipe with local wall thinning.

On the other hand, when the angle of wall thinning 2θ was 30°, as shown in Fig. 7c, API579-1 gave a good estimation and BS7910/ASME B31G provided lower

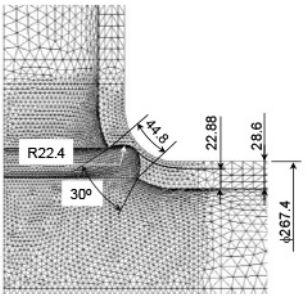

FIG. 8. — Geometry of local wall thinning with $T'/T = 0.2$ and $2\theta = 30°$.

*RSF*s than those estimated by FEA except for $T'/T = 0.2$. In case of $2\theta = 30°$ and $T'/T = 0.2$, all codes and standards gave higher *RSF*s than that by FEA. In order to recognise this behaviour, detailed geometry of local wall thinning for case number Tj-L9 with $2\theta = 30°$ and $T'/T = 0.2$ is shown in Fig. 8. The depth was deeper than the half-width estimated with the half-angle of local wall thinning. The applicability of acceptance standards for local wall thinning in API579-1 is limited to the following equation,

$$g_r > T\text{-}T' \tag{14}$$

where g_r is the radius at the base of a groove like flaw, which is half of the width of local wall thinning. Since the g_r was 22.4 mm and T-T' was 22.88 mm in case number Tj-L9, API 579-1 did not directly meet the applicability of the acceptance standards for local wall thinning.

Although the acceptance standards for local wall thinning in API579-1 could be applied to those of T-joint piping and BS7910/ASME B31G gave the conservative estimations for T- joint piping, the acceptance of deep and narrow wall thinning should be evaluated with FEA estimations.

V. Summary

In order to clarify the relevence of current acceptance standards to T-joint pipes with a fully circumferential local wall thinning subjected to internal pressure, the estimated failure pressures by FEA were compared with those estimated by the acceptance standards in worldwide fitness-for-service codes and standards.

Although the estimated failure pressures of T-joint pipes were much higher than the minimum allowable pressure estimated with the assumption of the constant minimum thickness in design code, the margin depended on the geometry of local wall thinning.

It was confirmed that the current acceptance standards of local wall thinning in API579-1 could be generally applied to those of T-joint piping and BS7910/ASME B31G gave more conservative estimations for T-joint piping. However, the acceptance of deep and narrow local wall thinning in a T-joint, whose geometric conditions were beyond the scope of limitations of acceptance standards for local wall thinning, should be evaluated with FEA estimations as shown in this paper.

References

1. JSME, "Codes for Nuclear Power Generation Facilities — Rules on Pipe Wall Thinning Management for PWR Power Plans", JSME S NG1-2006. Japan Society of Mechanical Engineers, Tokyo, Japan, 2006.
2. JSME, "Codes for Nuclear Power Generation Facilities — Rules on Pipe Wall Thinning Management for BWR Power Plans", JSME S NH1-2006. Japan Society of Mechanical Engineers, Tokyo, Japan, 2006.
3. API, "API 579-1/ASME FFS-1. Fitness-For-Service Assessment Standard". Third Edition. American Petroleum Institute, Washington, DC, 2016

4. BSI, "BS7910:2015. Guide to Methods for Assessing the Acceptability of Flaws in Metallic Structures". British Standards Institution, London, UK, 2015.
5. ASME, "B31G-2012. Manual for Determining the Remaining Strength of Corroded Pipelines". American Society of Mechanical Engineers, New York, NY, USA, 2012.
6. JSA, "JIS G 3456:2014. Carbon Steel Pipes for High Temperature Service", Japanese Standards Association, Tokyo, Japan, 2014.
7. ASTM, "A106/A106M. Standard Specification for Seamless Carbon Steel Pipe for High-Temperature Service". ASTM International, West Conshohocken, PA, USA, 2015.
8. K. Teshima, M. Ochi, S. Asada, K. Hojo, T. Suzuki, M. Kugimoto, "Comparison Between Pressure Tests and Simulations for Thickness Management of Wall Thinning T-Joints" *in* "Proceedings" American Society of Mechanical Engineers (ASME) 2012 Pressure Vessels and Piping Conference, Toronto, Ontario, Canada, 15th–19th July 2012. Volume 3, Design and Analysis, Paper No. PVP2012-78686, pp. 131–37.
9. ASME, "ASME Boiler and Pressure Vessel Code (BPVC), Section III — Rules for Construction of Nuclear Facility Components". American Society of Mechanical Engineers, New York, NY, USA, 2015.
10. ASME, "ASME Boiler and Pressure Vessel Code (BPVC), Section II — Materials, Part D: Properties". American Society of Mechanical Engineers, New York, NY, USA, 2015.

fesipublishing.org.uk

ISBN 978-0-9576730-7-6